

Bright X-ray pulsars as sources of MeV neutrinos in the sky

Aman Asthana^{1*}, Alexander A. Mushtukov^{2†}, Alexandra A. Dobrynina³ and Igor S. Ognev³

¹ *Coppell High School, 185 W Parkway Blvd, Coppell, TX 75019 Coppell, USA*

² *Astrophysics, Department of Physics, University of Oxford, Denys Wilkinson Building, Keble Road, Oxford OX1 3RH, UK*

³ *P.G. Demidov Yaroslavl State University, Sovetskaya 14, 150003 Yaroslavl, Russia*

11 April 2023

ABSTRACT

High mass accretion rate onto strongly magnetised neutron stars results in the appearance of accretion columns supported by the radiation pressure and confined by the strong magnetic field of a star. At mass accretion rates above $\sim 10^{19} \text{ g s}^{-1}$, accretion columns are expected to be advective. Under such conditions, a noticeable part of the total energy release can be carried away by neutrinos of a MeV energy range. Relying on a simple model of the neutrino luminosity of accreting strongly magnetised neutron stars, we estimate the neutrino energy fluxes expected from six ULX pulsars known up to date and three brightest Be X-ray transits hosting magnetised neutron stars. Despite the large neutrino luminosity expected in ULX pulsars, the neutrino energy flux from the Be X-ray transients of our Galaxy, SMC and LMC is dominant. However, the neutrino flux from the brightest X-ray transients is estimated to be below the isotropic background by two orders of magnitude at least, which makes impossible direct registration of neutrino emission from accreting strongly magnetised neutron stars nowadays.

Key words: accretion – accretion discs – X-rays: binaries – stars: neutron – stars: oscillations

1 INTRODUCTION

X-ray pulsars (XRP) are strongly magnetised neutron stars (NSs) in close binary systems (see, e.g., Mushtukov & Tsygankov 2022). Their emission in X-rays is caused by the accretion of matter from a companion star, which loses its mass via stellar wind or through the inner Lagrange point. A strong magnetic field in XRP affects the geometry of accretion flow directing it towards small regions located close to magnetic poles of a NS and details of the interaction between material and radiation (Harding & Lai 2006). The apparent luminosity of XRP covers orders of magnitude from $10^{32} \text{ erg s}^{-1}$ to $10^{41} \text{ erg s}^{-1}$. The brightest XRP belong to the recently discovered class of pulsating ultra-luminous X-ray sources (ULXs, see Bachetti et al. 2014; Israel et al. 2017a and Fabrika et al. 2021 for review). The relation between the actual and apparent luminosity in the brightest ULXs is still under debate. On one hand, extreme accretion onto a NS can cause strong outflows from accretion disc (Shakura & Sunyaev 1973), which naturally results in geometrical collimation of X-ray radiation (Poutanen et al. 2007; King 2009; King et al. 2017). According to some authors, the collimation of X-ray radiation can lead to the fact that in certain directions, the apparent luminosity of the ULXs has orders of magnitude higher than the actual one (King et al. 2017; King & Lasota 2020). On the other hand, the high pulsed fractions observed in pulsating ULXs largely excludes strong

geometrical beaming (Mushtukov et al. 2021; Mushtukov & Portegies Zwart 2023), which says in favour of a relatively small difference between the luminosities. The possible similarity between the actual and apparent luminosity in ULX hosting NSs is in agreement with the recent result of population synthesis models (Kuranov et al. 2020) and the analysis based on the observed luminosity function of high mass X-ray binaries (Mushtukov et al. 2015b).

High mass accretion rates ($\gtrsim 10^{17} \text{ g s}^{-1}$) onto the surface of magnetised NSs results in the appearance of radiation pressure dominated shock above the surface and accretion columns (Basko & Sunyaev 1976; Wang & Frank 1981; Mushtukov et al. 2015a,b) - structures supported by radiation pressure and confined by a strong magnetic field.

Under conditions of very high mass accretion rates ($\gtrsim 10^{19} \text{ g s}^{-1}$), accretion columns turn into advection dominated state when the typical time of photon diffusion from the flow becomes comparable or larger than the dynamical timescale of accretion process (Mushtukov et al. 2018). In this case, a large fraction of energy can turn into the production of electron-positron pairs (Mushtukov et al. 2019) and further neutrino emission due to the pair's annihilation (Kaminker et al. 1992b). As a result, the brightest XRP can be comparably bright in neutrinos.

The theory of neutrino emission from bright XRP requires the development of an accurate model of accretion column, which accounts for mechanisms of magnetic opacity (Suleimanov et al. 2022, 2023) and possibly deviations of accreting matter state from the thermodynamic equilibrium (see Discussion in Mushtukov et al. 2019). Nonetheless, some

* E-mail: amanasthana12345@gmail.com (AA)

† E-mail: alexander.mushtukov@physics.ox.ac.uk (AAM)

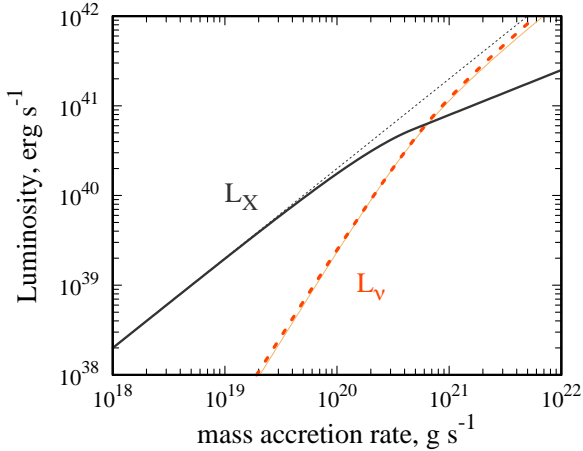


Figure 1. Dependence of X-ray (black solid line) and neutrino (red dashed line) luminosity on the mass accretion rate onto NS surface (Mushtukov et al. 2018). The solid orange line approximates neutrino luminosity according to (1). Total luminosity is given by the dotted black line. One can see that the total luminosity is dominated by photons at mass accretion rates $\lesssim 2 \times 10^{20} \text{ g s}^{-1}$. At higher mass accretion rates, neutrino luminosity becomes comparable to the photon luminosity and dominates at $\dot{M} \gtrsim 10^{21} \text{ g s}^{-1}$.

order of magnitude estimations can be done in the base of the toy model of the accretion column with advection (Mushtukov et al. 2018). The most promising candidates for the role of neutrino pulsars are pulsating ULXs (assuming their apparent luminosity is close to the actual one) and bright Be X-ray transients, which reach luminosity $\sim 10^{39} \text{ erg s}^{-1}$ at the peak of their outbursts (see Reig 2011 for review).

In this paper, we consider six pulsating ULXs known up to date - M82 X-2 (Bachetti et al. 2014), NGC 5907 X-1 (Israel et al. 2017a), NGC 7793 P13 (Fürst et al. 2016; Israel et al. 2017b), NGC 300 X-1 (Carpano et al. 2018), NGC 1313 X-2 (Sathyaprakash et al. 2019), and M51 X-7 (Rodríguez Castillo et al. 2020) - and three of the brightest Be X-ray transients: Swift J0243.6+6124 (Doroshenko et al. 2020), SMC X-3 (Tsygankov et al. 2017), and RX J0209.6-7427 (Vasilopoulos et al. 2020; Hou et al. 2022). Using a toy model of neutrino emission from accreting strongly magnetised NSs proposed by Mushtukov et al. 2018, we estimate the neutrino luminosity of considered objects and their corresponding neutrino energy flux at Earth. We compare the estimated flux level with the flux of neutrino background and sensitivity of neutrino telescopes.

2 MODEL

The estimation of neutrino luminosity and flux is based on the model proposed by Mushtukov et al. 2018. The model considers super-critical X-ray pulsars (Basko & Sunyaev 1976), where the luminosity of an accreting NS is high enough to support radiation pressure dominated accretion columns above NS magnetic poles. If the mass accretion rate onto a NS is high enough, the optical thickness of the accretion column prevents photon excitation from the accretion flow making the flow advective. Under these conditions, the internal temperature can increase up to a few hundred keV or

even a MeV. It results in the production of electron-positron pairs and further neutrino emission due to the pair's annihilation $e^-e^+ \rightarrow \nu\bar{\nu}$. Neutrinos produced due to the pair annihilation belong to the MeV energy band and are dominated initially (before accounting for neutrino oscillation) by electron neutrinos and anti-neutrinos. Neutrino synchrotron emission: $e^\mp \rightarrow e^\mp\nu\bar{\nu}$ also contributes to the total neutrino luminosity, but its contribution is expected to be relatively small (Kaminker et al. 1992a). The major uncertainty of the model is due to the fact that the model relies on the assumption that the concentration of electron-positron pairs is close to the equilibrium one. This condition may not be fulfilled in the accretion column because of short dynamical times of accretion ($\sim 10^{-4} \text{ s}$), which may be insufficient for the equilibrium concentration of the pairs (see discussion in Section 2 of Mushtukov et al. 2019). If the concentration of pairs is lower than the equilibrium concentration, the neutrino emission losses are also lower. Therefore, the estimates on which we rely should be regarded as optimistic. Uncertainties associated with the geometry of the accretion channel at the NS surface lead to uncertainties of the neutrino luminosity determination within a magnitude of 2–3.

The expected neutrino luminosity calculated under the assumption of the equilibrium pair concentration in the accretion channel can be approximated as

$$L_\nu \approx 0.64 L_{\text{tot}} \arctan\left(\frac{L_{\text{tot}}}{8 \times 10^{40} \text{ erg s}^{-1}}\right), \quad (1)$$

where $L_{\text{tot}} = L_X + L_\nu$ is the total luminosity of the source due to photon and neutrino emission (see Fig. 1 and more accurate results in Mushtukov et al. 2018).

Both photon and neutrino luminosity experience gravitational redshift. The luminosity in the observer's reference frame L_∞ is related to the luminosity at the surface of a NS of mass M and radius R as

$$L_\infty = L(1 - u), \quad (2)$$

where the compactness $u = R_S/R$, the Schwarzschild radius of a NS $R_S = 2GM/c^2 \approx 3 \times 10^5 (M/M_\odot) \text{ cm}$, and M_\odot is the mass of the Sun. The dependence of neutrino luminosity L_ν on the total luminosity L_{tot} is not linear (see Fig. 1). Thus, the procedure of neutrino luminosity estimation is divided into a few steps: (i) using the apparent photon luminosity of a NS we get the photon luminosity at the NS surface using (2), (ii) the photon luminosity at the NS surface is converted into neutrino luminosity at the NS using approximation (1) or more accurate estimations (Mushtukov et al. 2018), (iii) we get neutrino luminosity at the infinity accounting for the gravitational redshift (2). Because the apparent luminosity can be different from the actual one due to the geometrical beaming (King et al. 2017; Mushtukov et al. 2021), we illustrate the influence of this uncertainty assuming that the difference between two photon luminosities is within a factor of 2. With the known neutrino luminosity corrected for the gravitational redshift and distance to the source, we can estimate the expected neutrino energy flux at Earth.

3 ESTIMATIONS OF NEUTRINO LUMINOSITY

Estimating neutrino luminosity, we assume NS mass and radius to be $M = 1.4M_\odot$ and $R = 10^6 \text{ cm}$ respectively. All

Table 1. The table represents the maximal apparent X-ray luminosity of the objects L_X , expected neutrino luminosity L_ν , distance to the source, and corresponding neutrino energy flux F_ν at Earth from six pulsating ULXs discovered up to date and three bright Be XRPs. Estimations of neutrino luminosity are performed under the assumption that the apparent X-ray luminosity is equal to the actual one. NS mass and radius are taken to be $M = 1.4M_\odot$ and 10^6 cm respectively.

Name	L_X (max) [erg s ⁻¹]	L_ν [erg s ⁻¹]	D [ly]	F_ν [MeV cm ⁻² s ⁻¹]
NGC 5907 X-1	1.5×10^{41}	3.5×10^{41}	5.4×10^7	6.7×10^{-6}
NGC 1313 X-2	2×10^{40}	1.3×10^{40}	1.3×10^7	4.3×10^{-6}
M82 X-2	1.8×10^{40}	9×10^{39}	1.1×10^7	3.9×10^{-6}
M51 X-7	7×10^{39}	8.4×10^{38}	2.5×10^8	7.4×10^{-10}
NGC 7793 P13	5×10^{39}	4×10^{38}	1.2×10^7	1.5×10^{-7}
NGC 300 X-1	5×10^{39}	4×10^{38}	6×10^6	6×10^{-7}
SMC X-3	2.5×10^{39}	9×10^{37}	2×10^5	1.3×10^{-4}
Swift J0243.6+6124	2×10^{39}	5.7×10^{37}	1.64×10^4	1.2×10^{-2}
RX J0209.6-7427	1.1×10^{39}	1.7×10^{37}	2×10^5	2.3×10^{-5}

ULX pulsars are known to be strongly variable (see discussion on the observed variability in M82 X-2 by [Tsygankov et al. 2016](#), in NGC 5907 X-1 by [Israel et al. 2017a](#), in NGC 1313 X-2, M51 X-7, NGC 7793 P13 and NGC 300 X-1 by [Gürpide et al. 2021](#)) and our estimations of their neutrino luminosity and corresponding neutrino energy flux are based on the maximal detected X-ray luminosity.

The estimated neutrino luminosity and neutrino energy flux F_ν in six pulsating ULXs and in three bright Be X-ray transients at the peak of their outbursts are represented in Table 1. Despite relatively large neutrino luminosity expected in the ULXs, due to the difference in distance to the sources, the neutrino energy flux at Earth is below 10^{-5} MeV cm⁻² s⁻¹, which is smaller than the neutrino flux expected from considered Be X-ray transients.

By using recent observations of three bright X-ray transients - Swift J0243.6+6124, SMC X-3 and RX J0209.6-7427 - during their outbursts, we have obtained neutrino light curves during the outbursts (see blue squares in Fig. 2, 3 and 4). Because the neutrino luminosity is strongly dependent on the total luminosity of accreting NS, the uncertainties in estimations of actual X-ray luminosity result in significant uncertainties in estimations of neutrino luminosity and energy flux. Blue regions in Fig. 2, 3, 4 illustrate the uncertainty in neutrino luminosity due to the uncertainty in photons luminosity within a factor of 2. The majority of neutrinos are emitted during the main peak of the outbursts in Be XRP. When integrating the neutrino light curve obtained for three Be transients, we estimated the total energy emitted with neutrinos during the outbursts: $\sim 5 \times 10^{43}$ erg in Swift J0243.6+6124, $\sim 1.7 \times 10^{44}$ erg in SMC X-3, and $\sim 4.5 \times 10^{43}$ erg in RX J0209.6-7427.

The estimations of neutrino luminosity are dependent on NS mass and radius because of different contributions of the gravitational redshift. However, the uncertainties due to the unknown mass and radius of a NS are much smaller than the uncertainties due to the relation between the actual and apparent luminosity of the objects.

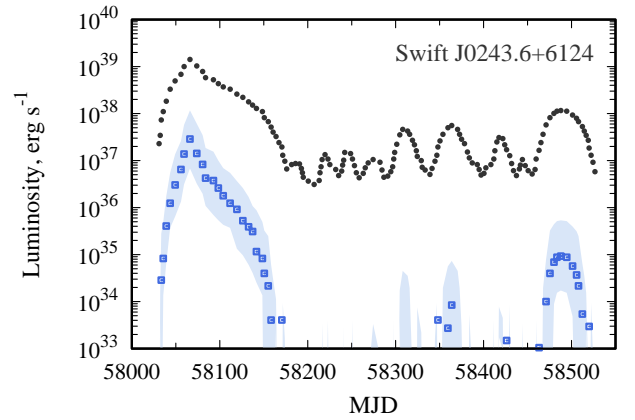


Figure 2. Black circles represent the photon light curve of Swift J0243.6+6124 during its outburst in 2017-2018 reproduced on the base of data from [Doroshenko et al. 2020](#), while blue squares represent neutrino light curve calculated on the base of [Mushtukov et al. 2018](#).

4 NEUTRINO FLUX PROPERTY AND DETECTION

4.1 Neutrino composition and energy spectrum

The possibility of neutrino detection at Earth is determined not only by the neutrino flux F_ν but also by neutrino species composition and their spectral distribution. The dominant process of neutrino emission from relatively hot electron-positron plasma is annihilation of electron-positron pairs (see, e. g., [Kaminker et al. 1992a](#)). The result of this reaction is production of neutrino and antineutrino of one of three flavors: electron ($\nu_e, \bar{\nu}_e$), muon ($\nu_\mu, \bar{\nu}_\mu$), or tau ($\nu_\tau, \bar{\nu}_\tau$). In the case of non-relativistic plasma and under the condition of extremely strong magnetic field $B \gg B_0 \approx 4.41 \times 10^{13}$ G, neutrino emissivity due to the annihilation is proportional to $c_V^2 + c_A^2$, while in the case of $B \ll B_0$, the emissivity of proportional to c_V^2 ([Kaminker et al. 1992b](#)). Here $c_V = \pm 1/2 + 2 \sin^2 \theta_W$ and $c_A = \pm 1/2$ are the vector and axial constants of the charged lepton current, and $\sin^2 \theta_W \approx 0.2312$, where θ_W is the Weinberg angle ([Workman & Others 2022](#)). The upper (plus) signs in c_V and c_A correspond to the electron flavor,

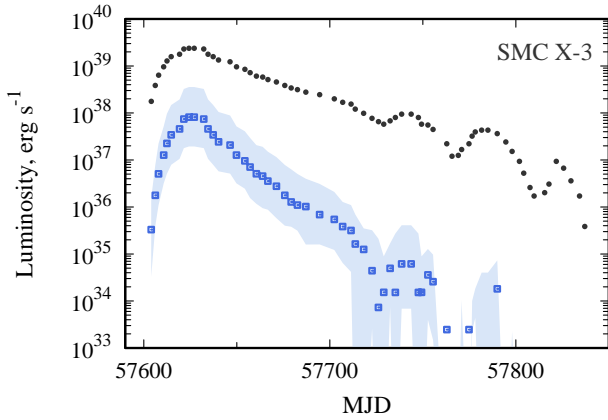


Figure 3. Black circles represent the photon light curve of SMC X-3 during its outburst in 2016-2017 reproduced on the base of data from [Tsygankov et al. 2017](#), while blue squares represent neutrino light curve calculated on the base of [Mushtukov et al. 2018](#).

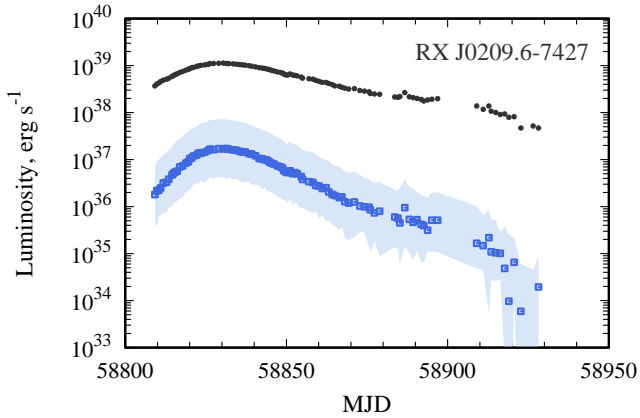


Figure 4. Black circles represent the photon light curve of RX J0209.6-7427 during its outburst in 2019-2020 reproduced on the base of data from [Hou et al. 2022](#), while blue squares represent neutrino light curve calculated on the base of [Mushtukov et al. 2018](#).

while the lower (minus) signs correspond to muon and tau species. So we could reconstruct the initial contributions of a different flavor to summarize neutrino luminosity L_ν . The initial electron neutrino and antineutrino luminosities are

$$L_{\nu_e} = L_{\bar{\nu}_e} \equiv f_{0e} L_\nu \quad (3)$$

and the initial muon/tau neutrino and antineutrino luminosities are

$$L_{\nu_\mu} = L_{\bar{\nu}_\mu} = L_{\nu_\tau} = L_{\bar{\nu}_\tau} \equiv f_{0x} L_\nu, \quad (4)$$

where $f_{0e} \approx 0.35$, $f_{0x} \approx 0.075$ for the case of magnetar-like magnetic field strength $B \gg B_0$, and $f_{0e} \approx 0.4985$, $f_{0x} \approx 0.00075$ for the case of relatively weak magnetic fields $B \ll B_0$ ([Kaminker et al. 1992b](#)). We neglect neutrino oscillation in the matter of X-ray source due to the essential uncertainty of accretion column geometry and its small extent. Gravitational redshift does not affect the flavor composition of neutrino flux.

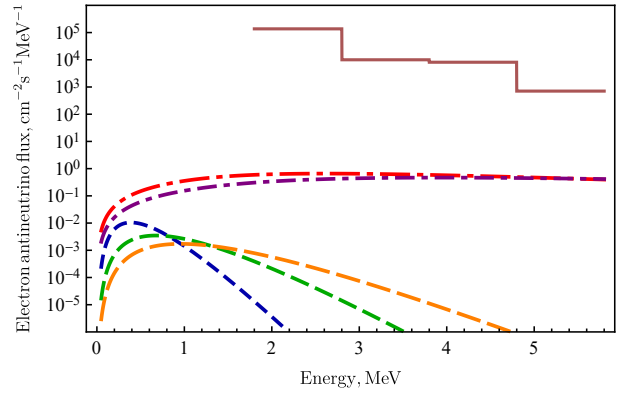


Figure 5. Set electron antineutrino fluxes $\varphi_{\bar{\nu}_e}$ as a function of energy. Swift J0243.6+6124: curves for different temperatures of neutrino emitted area $T_X = 0$ MeV (blue short dashed), $T_X = 0.25$ MeV (green dashed), $T_X = 0.5$ MeV (orange long dashed) Diffusion supernova background: pure neutron star $T_{SN} = 4$ MeV (red dot and long dash) and pure black hole $T_{SN} = 6$ MeV (purple dot and dash) forming. Borexino model-independent limit on electron antineutrino fluxes from unknown sources (brown solid).

However, neutrino propagation over the distance between the source and observer affects the composition of the flux due to the vacuum neutrino oscillations. The initial and final flavor fractions are related as ([Mena et al. 2007](#)):

$$\begin{aligned} f_e &= f_{0e} - (f_{0e} - f_{0x}) \sin^2(2\theta_{12})/2, \\ f_x &= f_{0x} - (f_{0e} - f_{0x}) \sin^2(2\theta_{12})/4, \end{aligned} \quad (5)$$

where $\sin^2 \theta_{12} \approx 0.307$ ([Workman & Others 2022](#)) is a squared sin of the neutrino mixing angle. Hence we obtain $f_e \approx 0.23$, $f_x \approx 0.135$ for magnetar-like accretor and $f_e \approx 0.29$, $f_x \approx 0.105$ for the accretor of weaker surface magnetic field. These values are equal approximately, so we used the following averages:

$$f_e = 1/4, \quad f_x = 1/8. \quad (6)$$

To restore the neutrino spectrum, we follow the result of paper by [Misiaszek et al. 2006](#). Possibility of neutrino detection could be obtained from the specific neutrino flux φ_ν , which has the dimension $[\varphi_\nu] = [\text{cm}^{-2} \text{s}^{-1} \text{MeV}^{-1}]$. The specific flux is related to neutrino energy flux F_ν as

$$F_\nu = \int_0^\infty \varepsilon \varphi_\nu(\varepsilon) d\varepsilon, \quad (7)$$

where ε is neutrino energy measured in MeV. Following the result of [Misiaszek et al. 2006](#), we approximate neutrino flux at Earth from an X-ray source as

$$\varphi_\nu(\varepsilon) = \frac{s^s F_\nu}{\Gamma(s) \bar{\varepsilon}^2} \left(\frac{\varepsilon}{\bar{\varepsilon}}\right)^{s-1} \exp\left(-s \frac{\varepsilon}{\bar{\varepsilon}}\right), \quad (8)$$

where the parameter $s \approx 4.181$ and the mean neutrino energy $\bar{\varepsilon} = m_e + 3/2 T_X$, T_X is the temperature of neutrino emitted medium and $m_e \approx 0.511$ MeV is electron mass. Note, that the spectra of different neutrino flavors are the same due to the kinematics of the annihilation process, and functions φ_{ν_i} corresponding to different flavors are differed from φ_ν by a factor f_e or f_x only (6).

The dependence of the neutrino spectrum on temperature is shown in Fig. 5. One can see that the spectrum of neutrino

emitted by hotter material is wider but lower at its maximum value.

4.2 Neutrinos detection

As seen from Table 1, pulsating ULXs have higher neutrino luminosity in comparison to three bright Be XRP considered in the paper. However, the neutrino energy flux at the Earth is smaller due to the large distance to ULXs. Below we discuss the possibility of neutrino detection Swift J0243.6+6124, which neutrino energy flux at the Earth is expected to be the highest one.

The observability of accreting NSs in neutrinos is determined by the sensitivity of neutrino telescopes and the ratio of neutrino flux from sources to the background. The sources of neutrino background can be isotropic and non-isotropic. Non-isotropic neutrino background in the energy band from 0.01 to 100 MeV is dominated by solar thermal and nuclear neutrinos (Fig. 6, A* and B* components), neutrinos from the ground based reactors (Fig. 6, C*) and geoneutrinos (Fig. 6, D*). The isotropic neutrino flux in the same energy band is due to neutrino emission of the nearest stars of the Galaxy (Fig. 6, E), old core-collapse supernova explosions (Fig. 6, F) and atmospheric neutrinos (Fig. 6, G).

Non-isotropic neutrino background is dominated over the isotropic background at a MeV energy range. Solar nuclear neutrino flux is estimated to be

$$F_{\odot} \gtrsim 10^8 \text{ MeV cm}^{-2} \text{ s}^{-1}.$$

Decay of radioactive isotopes in the Earth provides the flux of terrestrial antineutrinos (Dye 2012)

$$F_{\oplus} \sim 10^6 \text{ MeV cm}^{-2} \text{ s}^{-1}.$$

Nuclear reactors release a few percents of their total energy production in the form of MeV-range antineutrinos and cause the flux (Mueller et al. 2011)

$$F_{\text{nuc}} \sim F_{\oplus} \sim 10^6 \text{ MeV cm}^{-2} \text{ s}^{-1}.$$

Isotropic neutrino background (its components are shown by solid lines in Fig. 6) is a few orders of magnitude lower in comparison to the non-isotropic one. Ancient core collapse supernovae provide the neutrino flux

$$F_{\text{SN}} \sim 1 \text{ MeV cm}^{-2} \text{ s}^{-1}.$$

Neutrino flux from stars of the Galaxy is strongly dependent on energy (see curve E in Fig. 6) and direction: the isotropic component due to the neutrino emission by the nearest stars is estimated to be almost an order of magnitude smaller than the flux in the direction towards the Galactic center (Brocato et al. 1998). The composition of Galactic neutrinos is similar to the composition of neutrino flux from the Sun. The atmospheric neutrino and antineutrino flux due to interaction of cosmic rays with the atmosphere of Earth is estimated to be

$$F_{\text{atm}} < 10^{-2} \text{ MeV cm}^{-2} \text{ s}^{-1}$$

at a MeV energy range (Honda et al. 2015).

Detecting electron neutrinos from an X-ray source is difficult due to significant background from the Sun and Galactic stars. Thus, observation of accreting NSs is more preferred

in the other species of neutrino and antineutrino ($\nu_{\mu}/\bar{\nu}_{\mu}$ or $\nu_{\tau}/\bar{\nu}_{\tau}$). The most significant isotropic neutrino background of mixed flavours is provided by old core-collapse supernovae explosions, which are sources of all neutrino species. Although this background has an average energy of ~ 6 MeV, its estimated neutrino flux (Vitagliano et al. 2020):

$$\varphi_{\text{SN}}(\varepsilon) \approx 5.12 \left(\frac{4 \text{ MeV}}{T_{\text{SN}}} \right)^2 \arctan \left[3 \left(\frac{\varepsilon}{T_{\text{SN}}} \right)^{3/2} \right] \times e^{-1.03\varepsilon/T_{\text{SN}}} \quad (9)$$

exceed value corresponding to Swift J0243.6+6124. Supernova neutrino flavor composition is expected to be different for the explosions leading to production of NSs and black holes (Sumiyoshi et al. 2006; Walk et al. 2020). In the case of NS remnant, the flavour composition is given by $f_e \approx 1/4$, $f_x \approx 1/8$, and $T_{\text{SN}} \approx 4$ MeV, while in the case of black hole production neutrinos are dominated by the electron flavour: $f_e \approx 2/5$, $f_x \approx 1/20$, and $T_{\text{SN}} \approx 6$ MeV (Vitagliano et al. 2020). As one can see from the Fig. 5, the diffusion supernova background is in excess of the electron antineutrino emission from Swift J0243.6+6124 even in a MeV energy band. A similar result is for other neutrino species. Thus, old core-collapse supernova could produce significant background even for the brightest in neutrino X-ray source Swift J0243.6+6124.

Detection of MeV neutrinos and antineutrinos requires use of underground detectors. Further, we estimate the possibility of neutrino detection from X-ray sources using data from the Borexino underground detector (Alimonti et al. 2009). We use a model-independent upper limit in the energy range 1.8 – 16.8 MeV on electron antineutrino fluxes from unknown sources Agostini et al. (2021). In this paper, the monochromatic neutrinos model with 1 MeV wide bins was used, so the upper limit is a piecewise function. The result is shown in Fig. 5. As one can see from the picture, the Borexino model-independent limit exceeds electron antineutrino flux from Swift J0243.6+6124 by more than eight orders of magnitude. Note that the Borexino limit obtains through detector neutrino events of inverse beta decay of the free proton. The energy threshold of this reaction is 1.8 MeV, so the maximum neutrino spectrum from X-ray sources occurs in the lower energy range. Therefore the reaction of neutrino electron scattering is preferable for the detection of neutrinos from an X-ray source. Moreover, all neutrino species are involved in this reaction, in contrast to the inverse beta decay, where only the electron antineutrino participates. All backgrounds except old supernovae are electron neutrinos or antineutrinos. Thus, muon and tau (anti)neutrinos detection is the preferable strategy for the detection of neutrino signal from bright XRPs.

As discussed above, even neutrino brightest X-ray pulsar Swift J0243.6+6124 has the flux (i) under the background of diffuse neutrino from old supernovae, and (ii) significantly less than the reliable threshold of neutrino detection by existent detectors. Finally, we estimate the possibility of neutrino detection from near the Earth but unknown at present X-ray sources. For this purpose, we obtain the following simple approximation data from Table 1: $L_{\nu} \approx 1.6 \times 10^{39} (L_X/10^{40} \text{ erg s}^{-1})^2$. Note that approximation values differ from data less than 50 %. Hence we obtain an estimation of the distance on which neutrinos from the X-ray

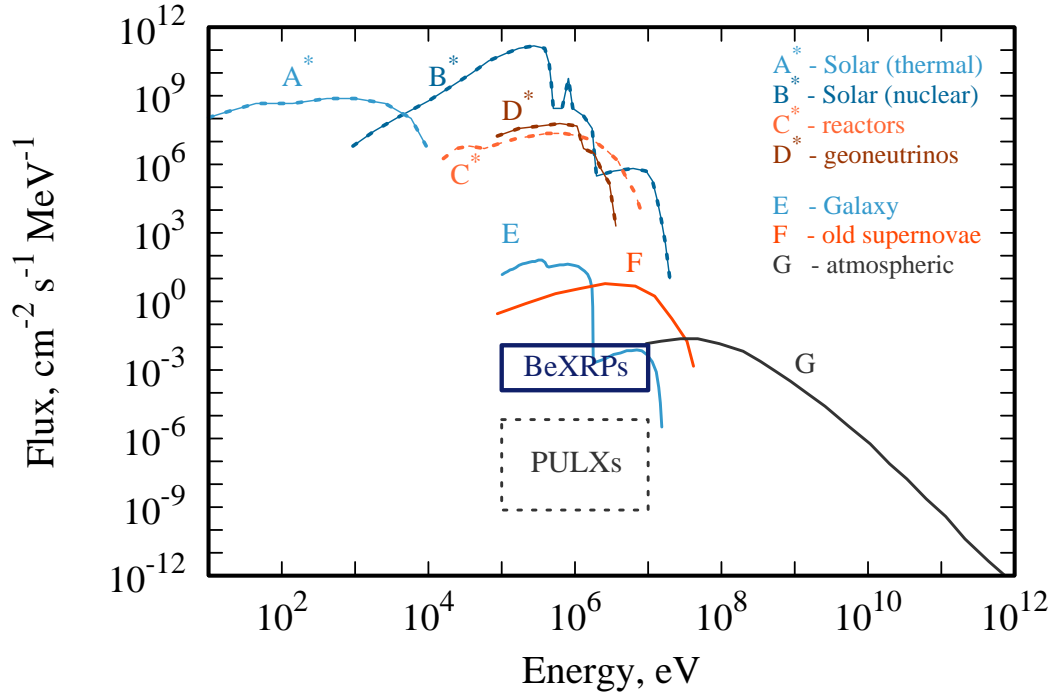


Figure 6. The energy spectrum of neutrino background at Earth summed over flavors in the energy range from 10 eV to 10^{12} eV (taken from Vitagliano et al. 2020 and Brocato et al. 1998). The background is composed of solar thermal (A^*) and nuclear neutrinos (B^*), neutrinos from nuclear reactors (C^*), geoneutrinos (D^*), isotropic component of neutrino flux from stars of the Galaxy (E), neutrinos from old supernovae (F), and atmospheric neutrinos (G). Dashed lines represent non-isotropic neutrino background, while the background represented by solid lines is expected to be isotropic. Note, that the total neutrino flux due to the stars of the Galaxy is not isotropic and expected to be larger (by a factor ~ 8 in comparison to the isotropic component) in the direction towards the Galactic center (see Fig. 8 in Brocato et al. 1998). Two rectangles show the area, where we expect neutrino flux from three bright BeXRPs at the peak of their outbursts (solid blue) and from six pulsating ULXs (dashed black).

sources could be detected at the maximum of their spectrum:

$$D_* \sim \left(\frac{10^5 \text{ cm}^{-2} \text{ s}^{-1} \text{ MeV}^{-1}}{\varphi_{th}} \right)^{1/2} \left(\frac{L_X}{10^{39} \text{ erg s}^{-1}} \right) \text{ ly}, \quad (10)$$

where φ_{th} is threshold of detection neutrino flux. It follows from the estimation that Be XRPs, able to be detected by existent neutrino telescope, should be located among the nearest stars. Whereas pulsating ULXs could be detected from a distance of a few hundred light years. Note that a special method of selecting neutrino events in the detector, such as taking into account the direction of X-ray sources, detection muon and tau (anti)neutrinos, could decrease the detection threshold and increase the distance to the detectable X-ray objects.

5 SUMMARY

In this paper, we have considered accreting strongly magnetized NSs as possible sources of neutrino emission. Applying the model proposed by Mushtukov et al. 2018 to six ULX pulsars and three bright Be XRPs, we have estimated neutrino luminosity and neutrino energy flux from these objects (see Table 1). Despite the large total neutrino luminosity of ULX pulsars, the neutrino energy flux from the Be X-ray transients of our Galaxy (Swift J0243.6+6124) and Magellanic Clouds (SMC X-3 and RX J0209.6-7427) is expected to be

dominant due to a relatively small distance from them. For the case of Be XRPs, we have provided the expected neutrino light curve during their recent outbursts (see Fig. 2, 3 and 4). The total energy release due to the neutrino emission during the outbursts was estimated to be at the level of 10^{44} erg.

Because the major process of neutrino emission in bright XRPs is the annihilation of electron-positron pairs, the flux is composed equally of neutrinos and antineutrinos of a MeV energy range, where about a half of particles belong to the electron flavour. In a MeV energy range, the neutrino background is dominated by non-isotropic sources: solar neutrinos, antineutrinos from nuclear reactors and terrestrial antineutrinos due to the decay of radioactive isotopes (B^* , C^* , D^* curves in Fig. 6 respectively). Isotropic neutrino background is a few orders of magnitude lower and in a MeV energy range dominated by neutrinos/antineutrinos from old core-collapse supernova explosions and neutrinos from the nearest stars of the Galaxy (F and E curves in Fig. 6 respectively). Because there is a lack of antineutrinos in the flux from the Sun and stars of the Galaxy, it is preferable to observe accreting NSs in antineutrinos. However, the flux from bright Be X-ray transients considered in our paper is still more than two orders of magnitude below the isotropic neutrino background due to old supernova explosions (see Fig. 6). Therefore, direct registration of neutrino emission from accreting NSs seems impossible at present and confirmation of significant energy

losses with neutrino by NSs requires the development of indirect methods.

ACKNOWLEDGEMENTS

AAM thanks UKRI Stephen Hawking fellowship. We are grateful to an anonymous referee for useful comments and suggestions.

DATA AVAILABILITY

The calculations presented in this paper were performed using a private code developed and owned by the corresponding author. All the data appearing in the figures are available upon request.

REFERENCES

- Agostini M., et al., 2021, *Astropart. Phys.*, 125, 102509
- Alimonti G., et al., 2009, *Nuclear Instruments and Methods in Physics Research A*, 600, 568
- Bachetti M., et al., 2014, *Nature*, 514, 202
- Basko M. M., Sunyaev R. A., 1976, *MNRAS*, 175, 395
- Brocato E., Castellani V., degl'Innocenti S., Fiorentini G., Raimondo G., 1998, *A&A*, 333, 910
- Carpano S., Haberl F., Maitra C., Vasilopoulos G., 2018, *MNRAS*, 476, L45
- Doroshenko V., et al., 2020, *MNRAS*, 491, 1857
- Dye S. T., 2012, *Reviews of Geophysics*, 50, RG3007
- Fabrika S. N., Atapin K. E., Vinokurov A. S., Sholukhova O. N., 2021, *Astrophysical Bulletin*, 76, 6
- Fürst F., et al., 2016, *ApJ*, 831, L14
- Gúrpide A., Godet O., Koliopanos F., Webb N., Olive J. F., 2021, *A&A*, 649, A104
- Harding A. K., Lai D., 2006, *Reports on Progress in Physics*, 69, 2631
- Honda M., Athar M. S., Kajita T., Kasahara K., Midorikawa S., 2015, *Phys. Rev. D*, 92, 023004
- Hou X., et al., 2022, *ApJ*, 938, 149
- Israel G. L., et al., 2017a, *Science*, 355, 817
- Israel G. L., et al., 2017b, *MNRAS*, 466, L48
- Kaminker A. D., Levenfish K. P., Yakovlev D. G., Amsterdamski P., Haensel P., 1992a, *Phys. Rev. D*, 46, 3256
- Kaminker A. D., Gnedin O. Y., Yakovlev D. G., Amsterdamski P., Haensel P., 1992b, *Phys. Rev. D*, 46, 4133
- King A. R., 2009, *MNRAS*, 393, L41
- King A., Lasota J.-P., 2020, *MNRAS*, 494, 3611
- King A., Lasota J.-P., Kluźniak W., 2017, *MNRAS*, 468, L59
- Kuranov A. G., Postnov K. A., Yungelson L. R., 2020, *Astronomy Letters*, 46, 658
- Mena O., Mocioiu I., Razzaque S., 2007, *Phys. Rev. D*, 75, 063003
- Misiaszek M., Odrzywolek A., Kutschera M., 2006, *Phys. Rev. D*, 74, 043006
- Mueller T. A., et al., 2011, *Phys. Rev. C*, 83, 054615
- Mushtukov A. A., Portegies Zwart S., 2023, *MNRAS*, 518, 5457
- Mushtukov A., Tsygankov S., 2022, arXiv e-prints, p. arXiv:2204.14185
- Mushtukov A. A., Suleimanov V. F., Tsygankov S. S., Poutanen J., 2015a, *MNRAS*, 447, 1847
- Mushtukov A. A., Suleimanov V. F., Tsygankov S. S., Poutanen J., 2015b, *MNRAS*, 454, 2539
- Mushtukov A. A., Tsygankov S. S., Suleimanov V. F., Poutanen J., 2018, *MNRAS*, 476, 2867
- Mushtukov A. A., Ognev I. S., Nagirner D. I., 2019, *MNRAS*, 485, L131
- Mushtukov A. A., Portegies Zwart S., Tsygankov S. S., Nagirner D. I., Poutanen J., 2021, *MNRAS*, 501, 2424
- Poutanen J., Lipunova G., Fabrika S., Butkevich A. G., Abolmasov P., 2007, *MNRAS*, 377, 1187
- Reig P., 2011, *Ap&SS*, 332, 1
- Rodríguez Castillo G. A., et al., 2020, *ApJ*, 895, 60
- Sathyaprakash R., et al., 2019, *MNRAS*, 488, L35
- Shakura N. I., Sunyaev R. A., 1973, *A&A*, 24, 337
- Suleimanov V. F., Mushtukov A. A., Ognev I., Doroshenko V. A., Werner K., 2022, *MNRAS*, 517, 4022
- Suleimanov V. F., Mushtukov A., Ognev I., Doroshenko V. A., Werner K., 2023, *IAU Symposium*, 363, 327
- Sumiyoshi K., Yamada S., Suzuki H., Chiba S., 2006, *Phys. Rev. Lett.*, 97, 091101
- Tsygankov S. S., Mushtukov A. A., Suleimanov V. F., Poutanen J., 2016, *MNRAS*, 457, 1101
- Tsygankov S. S., Doroshenko V., Lutovinov A. A., Mushtukov A. A., Poutanen J., 2017, *A&A*, 605, A39
- Vasilopoulos G., et al., 2020, *MNRAS*, 494, 5350
- Vitagliano E., Tamborra I., Raffelt G., 2020, *Rev. Mod. Phys.*, 92, 45006
- Walk L., Tamborra I., Janka H.-T., Summa A., Kresse D., 2020, *Phys. Rev. D*, 101, 123013
- Wang Y. M., Frank J., 1981, *A&A*, 93, 255
- Workman R. L., Others 2022, *PTEP*, 2022, 083C01

This paper has been typeset from a $\text{\TeX}/\text{\LaTeX}$ file prepared by the author.